optica

Microwave-to-optical conversion using lithium niobate thin-film acoustic resonators

LINBO SHAO[1,6], MENGJIE YU[1], SMARAK MAITY[1], NEIL SINCLAIR[1,2], LU ZHENG[3], CLEAVEN CHIA[1], AMIRHASSAN SHAMS-ANSARI[1], CHENG WANG[1,4], MIAN ZHANG[1,5], KEJI LAI[3], AND MARKO LONČAR[1,7]

[1]John A. Paulson School of Engineering and Applied Sciences, Harvard University, 29 Oxford Street, Cambridge, Massachusetts 02138, USA
[2]Division of Physics, Mathematics and Astronomy, and Alliance for Quantum Technologies (AQT), California Institute of Technology, 1200 E. California Blvd., Pasadena, California 91125, USA
[3]Department of Physics, University of Texas at Austin, Austin, Texas 78712, USA
[4]Department of Electrical Engineering & State Key Laboratory of THz and Millimeter Waves, City University of Hong Kong, Kowloon, Hong Kong, China
[5]HyperLight Corporation, 501 Massachusetts Avenue, Cambridge, Massachusetts 02139, USA
[6]e-mail: shaolb@seas.harvard.edu
[7]e-mail: loncar@seas.harvard.edu

Published 2 December 2019

This document provides supplementary information to "Microwave-to-optical conversion using lithium niobate thin-film acoustic resonators," https://doi.org/10.1364/OPTICA.6.001498. It provides details of numerical simulations of acousto-optic interactions, dynamics of the acousto-optic cavity, and calculations of the acousto-optic coupling and conversion efficiencies.

1. NUMERICAL SIMULATION OF THE ACOUSTO-OPTIC INTERACTION

We perform a 2D numerical simulation of our device cross-section (Fig. S1(a)) using COMSOL Multiphysics. Optical and acoustic modes are simulated independently and the acousto-optic interactions are then calculated by the integral of acoustic and optical fields using corresponding nonlinear coefficient matrices.

A. Simulation of optical and acoustic modes

The single-mode optical waveguide of our device supports fundamental TE and TM modes (Fig. S1). The electric field profiles of the optical modes are used in the calculation of the acousto-optic interaction.

The simulation of the acoustic mode includes strain, electric field, and the piezoelectric effect. Multiple acoustic modes with gigahertz resonant frequencies are found in the eigenmode simulation. We plot only a few acoustic modes in Fig. S2. The electrical excitation of these acoustic modes are enabled by the interdigital transducers (IDTs).

B. Calculation of acousto-optic interactions

The acousto-optic interactions are calculated by integrating the optical and acoustic modes with matrices that describe moving boundary, photoelastic and electro-optic effects. Calculations here are based on theory formulated in previous works [1–4].

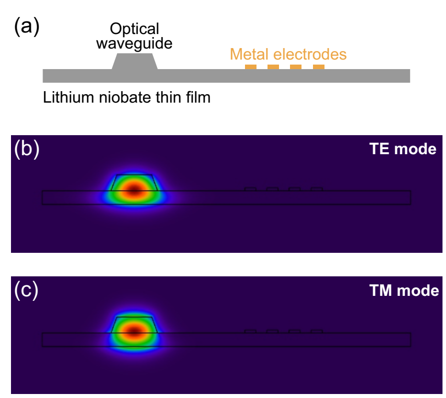

Fig. S1. (a) Device structure for 2D numerical simulation. (b), (c) Optical electric field of the fundamental TE and TM modes, respectively.

In our work, the acousto-optic interactions are described by the change of optical mode index due to the acoustic mode. The acoustic mode amplitude α, defined by the maximum displacement, is normalized to a single phonon occupation of the acoustic resonator using $\hbar\Omega = \frac{1}{2}m_{\mathrm{eff}}\Omega^2\alpha^2$, where Ω is the acoustic frequency. The effective mass m_{eff} of the acoustic mode is

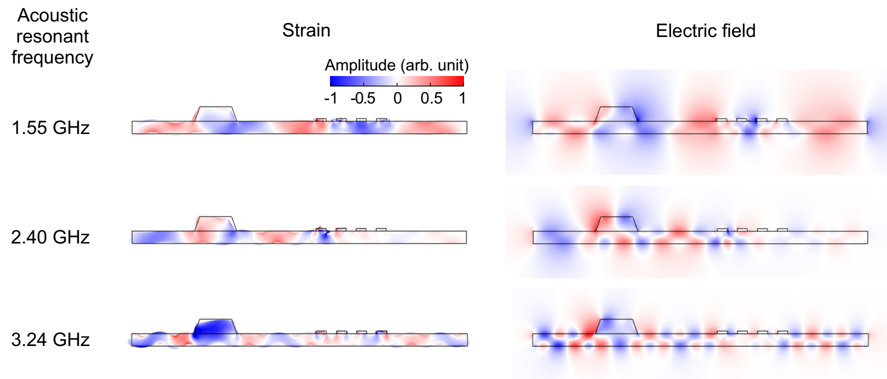

Fig. S2. Strain and electric field of three simulated acoustic modes with resonant frequencies of 1.55, 2.40, and 3.24 GHz. The color map is independently normalized for each simulation.

given by

$$m_{\text{eff}} = L_a \int_D \rho\, Q(\mathbf{r})^2 d\mathbf{r} / \max_D \left(Q(\mathbf{r})^2\right), \tag{S1}$$

where D defines the 2D simulation domain and the coordinate variable $\boldsymbol{r} \in D$. L_a is the length (perpendicular to the simulation cross-section) of the acoustic resonator, ρ is material mass density, and Q is the displacement field.

The electric field of the optical mode is denoted as E, s refers to strain, and $\mathcal{E}$ refers to the electric field of the acoustic mode. The mode index modulated by the moving boundary effect is given by

$$\Delta n_{0,\text{MB}} = -\frac{n}{2}\frac{\oint (Q\cdot\hat{\mathbf{n}})\left(E_\parallel^*\Delta\epsilon E_\parallel - D_\perp^*\Delta\epsilon^{-1}D_\perp\right)dS}{\int E^*\epsilon E dr}, \tag{S2}$$

where n is the optical mode index, $\hat{\mathbf{n}}$ is the normal vector of the boundary facing outward, and D is the electric displacement field of the optical mode. The subscripts $\parallel$ and $\perp$ indicate the parallel and perpendicular components to the boundary. The permittivity for the optical electric field is denoted as ϵ, while $\Delta\epsilon = \epsilon_{\text{LN}} - \epsilon_{\text{air}}$, and $\Delta\epsilon^{-1} = \epsilon_{\text{LN}}^{-1} - \epsilon_{\text{air}}^{-1}$.

The mode index modulated by the photoelastic effect is given by

$$\Delta n_{0,\text{PE}} = \frac{\epsilon_0 n^5}{2}\frac{\int dr \begin{pmatrix} E_x^* & E_y^* & E_z^* \end{pmatrix}\begin{pmatrix} dB_1 & dB_6 & dB_5 \\ dB_6 & dB_2 & dB_4 \\ dB_5 & dB_4 & dB_3 \end{pmatrix}\begin{pmatrix} E_x \\ E_y \\ E_z \end{pmatrix}}{\int E^*\epsilon E dr}, \tag{S3}$$

where ϵ_0 is the vacuum permittivity, and B_k $(k = 1-6)$ is the optical indicatrix. The changes of indicatrix coefficient dB_k $(k = 1-6)$ due to the strain s_k $(k = 1-6)$ is given by

$$\begin{pmatrix} dB_1 \\ dB_2 \\ dB_3 \\ dB_4 \\ dB_5 \\ dB_6 \end{pmatrix} = \begin{pmatrix} p_{33} & p_{31} & p_{31} & 0 & 0 & 0 \\ p_{13} & p_{11} & p_{12} & 0 & p_{14} & 0 \\ p_{13} & p_{12} & p_{11} & 0 & -p_{14} & 0 \\ 0 & 0 & 0 & p_{66} & 0 & p_{14} \\ 0 & p_{41} & -p_{41} & 0 & p_{44} & 0 \\ 0 & 0 & 0 & p_{41} & 0 & p_{44} \end{pmatrix}\begin{pmatrix} s_1 \\ s_2 \\ s_3 \\ s_4 \\ s_5 \\ s_6 \end{pmatrix}. \tag{S4}$$

where p_{jk} are the primary elasto-optic coefficients in the condition of a constant electric field for lithium niobate (LN), where the secondary effect via piezoelectricity and electro-optics is excluded [5, 6]. The photoelastic matrix is rotated according to the crystal orientation in our device – X-cut thin-film LN with acoustic wave propagating in the Z direction of the crystal. The coordinate representations for the simulation and crystal are shown in Fig. 2(a).

The mode index modulated by the electro-optic effect $\Delta n_{0,\text{EO}}$ is of the same form of Eq. S3, with the changes of indicatrix coefficients [4] given by

$$\begin{pmatrix} dB_1 \\ dB_2 \\ dB_3 \\ dB_4 \\ dB_5 \\ dB_6 \end{pmatrix} = \begin{pmatrix} r_{33} & 0 & 0 \\ r_{13} & 0 & -r_{22} \\ r_{13} & 0 & r_{22} \\ 0 & -r_{22} & 0 \\ 0 & 0 & r_{51} \\ 0 & -r_{51} & 0 \end{pmatrix}\begin{pmatrix} \mathcal{E}_x \\ \mathcal{E}_y \\ \mathcal{E}_z \end{pmatrix}, \tag{S5}$$

where r_{jk} is the primary electro-optic coefficients in the condition of constant strain in which secondary effects via piezoelectricity and photoelasticity is excluded. The above matrix is rotated according to the crystal orientation in our device.

The overall relative refractive index change due to a single phonon is given by,

$$\Delta n_{0,\text{tot}} = \Delta n_{0,\text{MB}} + \Delta n_{0,\text{PE}} + \Delta n_{0,\text{EO}}. \tag{S6}$$

C. Calculation of $V_\pi L$

The half-wave-voltage-length product $V_\pi L$, characterizing the modulation efficiency, defines the voltage that is required to achieve a π phase shift for a modulation length L. Here, we derive the $V_\pi L$ from the simulated refractive index changes with additional information on Q factors and coupling of the acoustic resonator. While the overall refractive index change in Eq. S6 quantifies the optical phase shift (or index change) due to a single phonon in the acoustic resonator, one must relate the in-cavity phonon number to the applied microwave power. As discussed later in Sec. 3, the in-cavity phonon number is given by

$$N_{pn} = \frac{4\gamma_e}{\gamma^2} N_{in} = \frac{4\gamma_e}{\gamma^2}\frac{P_{in}}{\hbar\Omega_m}, \tag{S7}$$

Table S1. Numerical simulation results of acousto-optic interactions

Optical mode	Acoustic mode freq.	$\Delta n_{0,\mathrm{MB}}$	$\Delta n_{0,\mathrm{PE}}$	$\Delta n_{0,\mathrm{EO}}$	$\Delta n_{0,\mathrm{tot}}$	MZI		AO cavity
						$V_\pi L$	V_π	g_0
	GHz	$\times 10^{-12}$	$\times 10^{-12}$	$\times 10^{-12}$	$\times 10^{-12}$	V·cm	V	kHz
TE	1.55	0.36	1.40	30.5	32.26	0.0692	6.92	0.5
TE	2.17	-0.84	1.11	71.43	71.70	0.0436	4.36	1.1
TE	2.40	-0.80	-5.08	23.06	17.17	0.2009	20.1	0.27
TE	3.16	-3.07	41.68	26.38	64.99	0.0703	7.03	1.0
TE	3.24	-4.24	47.84	58.91	102.5	0.0454	4.54	1.6
TM	1.55	4.19	24.29	-8.79	19.69	0.113	11.3	0.3
TM	2.17	8.39	67.97	-24.03	52.33	0.0599	5.99	0.8
TM	2.40	0.87	22.26	-9.37	13.72	0.2505	25.1	0.2
TM	3.16	15.09	42.06	-4.28	52.87	0.0863	8.63	0.8
TM	3.24	21.03	70.63	-15.75	75.90	0.0616	6.16	1.2

where $N_{in} = P_{in}/\hbar\Omega_m$ is the phonon input rate with the resonant frequency Ω_m of the acoustic mode and input power P_{in}. The decay are and external coupling rates of the acoustic mode is γ and γ_e, respectively. Given the input impedance $R_{in} = 50\Omega$, the relation between input power and peak voltage V_p is given by

$$P_{in} = \frac{1}{2}\frac{V_p^2}{R_{in}}. \tag{S8}$$

The number of in-cavity phonons N_{pn} required for a π phase shift is given by,

$$\frac{2\pi}{\lambda}\Delta n_{0,\mathrm{tot}}\sqrt{N_{pn}}L = \pi \tag{S9}$$

where λ is the optical wavelength. Taking Eqs. S7 and S8 in to Eq. S9, we derive the $V_\pi L$ of the device:

$$V_\pi L = \frac{\lambda}{2\Delta n_{0,\mathrm{tot}}}\sqrt{\frac{\gamma^2\hbar\Omega_m R_{in}}{2\gamma_e}}. \tag{S10}$$

D. Calculation of acousto-optic single-photon coupling strength g_0

For our thin-film acoustic resonator that is coupled to an optical racetrack cavity, the acousto-optic single-photon coupling strength g_0 can be derived using the 2D simulation results using

$$g_0 = \omega_0 \eta_{\mathrm{cav}} \frac{\Delta n_{0,\mathrm{tot}}}{n}, \tag{S11}$$

where ω_0 is the optical resonant frequency, and η_{cav} is the ratio of waveguide length in the acoustic resonator to that of the racetrack cavity.

E. Estimate $V_\pi L$ and g_0 using the numerical simulation results

We estimate the $V_\pi L$ for the Mach–Zehnder interferometer (MZI) and g_0 for the acousto-optic cavity from simulation. To be consistent with the experiments, the typical measured acoustic Q factors $Q_m = 2{,}000$ ($\gamma = \Omega_m/Q_m$) and $\gamma_e/\gamma = 0.15$ (corresponding to a 3 dB dip in S_{11} measurements) are employed in the following calculation. The length of the acoustic resonator (in direction perpendicular to the simulation cross-section) is $L_a = 100\ \mu$m. The output impedance of the microwave source is $R_{in} = 50\ \Omega$. For the acoustic-optic cavity shown in Fig. 1, the relative length of the optical waveguide in the acoustic resonator is $\eta_{\mathrm{cav}} = 0.15$. Table S1 summarizes the interactions between optical modes and acoustic modes.

2. DERIVATION OF V_π FROM EXPERIMENTAL MEASUREMENTS

A. Acousto-optic Mach-Zehnder interferometer

Here we relate the half-wave voltage V_π to the measured opto-acoustic S_{21} for the acousto-optic MZI. The phase modulation of one optical path is given by

$$E_{p1}(V) = \frac{E_0}{\sqrt{2}}\exp\left(i\pi V/V_\pi + i\phi_b\right), \tag{S12}$$

where E_0 is the input optical field of the MZI, ϕ_b is the bias phase between two optical paths, and V is the applied voltage. The other optical path of MZI is not modulated, and the optical field is given by $E_{p2}(V) = E_0/\sqrt{2}$. The optical field at the output of the MZI is given by

$$\begin{aligned} E_{\mathrm{out}}(V) &= \frac{E_{p1}(V) + E_{p2}(V)}{\sqrt{2}} \\ &= \frac{E_0}{2}\left(1 + \exp\left(i\pi V/V_\pi + i\phi_b\right)\right). \end{aligned} \tag{S13}$$

The output optical power is thus given by

$$\begin{aligned} I_{\mathrm{out}}(V) &\propto E^*_{\mathrm{out}} E_{\mathrm{out}} \\ &= \frac{|E_0|^2}{2}\left(1 + \cos\left(\pi V/V_\pi + \phi_b\right)\right). \end{aligned} \tag{S14}$$

The optimum microwave to optical conversion occurs at the bias phase $\phi_b = \pi/2$, which corresponds to the output intensity at half maximum. Measured using a potodetector, the opto-acoustic S_{21} for small input signal is given by

$$S_{21} = \left(\frac{\pi R_{PD}\, I_{\text{rec}}}{V_\pi}\right)^2, \tag{S15}$$

where I_{rec} is the DC optical power received at the photodetector, and R_{PD} is sensitivity of the photodetector. Using Eq. S15, we can derive V_π of the acousto-optic MZI by the opto-acoustic S_{21} measurements.

B. Acousto-optic cavity

Our acousto-optic cavity operates in the sideband resolved regime, that is the frequency of the microwave signals are greater than the decay rate of the optical mode. For a weak microwave signal, the optical transmission is thus close to unitary at the optimum conversion wavelength, which corresponds to that detuned from the optical resonance by the microwave frequency. Phenomenologically, this can be understood as the light being reversibly pumped into, and out of, the optical cavity due to the acoustic modulation. Thus, we consider the acousto-optic cavity as an intensity modulator and the relation in Eq. S15 is also used to derive the effective V_π.

3. CONVERSION BETWEEN MICROWAVE, ACOUSTIC, AND OPTICAL FIELDS IN ACOUSTO-OPTIC CAVITY

A. Dynamics of acousto-optic cavity

Here we consider an acousto-optic system with an acoustic resonator driven by a microwave signal through the piezoelectric effect. The Heisenberg-Langevin equations of motion for an optical cavity a coupled to an acoustic resonator b are given by

$$\dot{a} = -\left(i\Delta + \frac{\kappa}{2}\right) a - i g_0 a \left(b + b^\dagger\right) + \sqrt{\kappa_e} a_{in} \tag{S16}$$

$$\dot{b} = -\left(i\Omega_m + \frac{\gamma}{2}\right) b - i g_0 a^\dagger a + \sqrt{\gamma_e} b_{in}, \tag{S17}$$

where a and b are the annihilation operators of optical and acoustic modes, respectively, g_0 is the single-photon coupling strength between the optical and acoustic resonators, $\Delta = \omega_0 - \omega_p$ is the optical detuning with the pump laser frequency ω_p, the optical resonant frequency is ω_0, $\kappa = \kappa_i + \kappa_e$ is the loss of optical mode with intrinsic loss κ_i and external coupling rate κ_e, Ω_m is the acoustic resonant frequency, $\gamma = \gamma_i + \gamma_e$ is the loss of acoustic mode with intrinsic loss γ_i and external coupling rate γ_e, and a_{in} and b_{in} are the optical and microwave input field, respectively.

To solve the equations of motion, we consider a single frequency microwave driving b_{in} of the acoustic resonator given by

$$b_{in} = B_{in} e^{-i\Omega_d t}, \tag{S18}$$

where Ω_d is the driving frequency, B_{in} is the amplitude of the input field, and the input microwave power is $P_{in} = \hbar\Omega_m \left|B_{in}\right|^2$. In the weak optical mode limit, i.e. $g_0 a^\dagger a \ll \Omega_m$, the optical back action term ($i g_0 a^\dagger a$ in Eq. S17) on the acoustic resonator is neglected. Taking Eq. S18 into Eq. S17, the acoustic amplitude b is solved using

$$\begin{aligned} b &= B e^{-i\Omega_d t} \\ B &= \frac{\sqrt{\gamma_e}}{i\left(\Omega_m - \Omega_d\right) + \frac{\gamma}{2}} B_{in}. \end{aligned} \tag{S19}$$

For a resonant microwave drive ($\Omega_m = \Omega_d$), the in-resonator phonon number N_{pn} is related to the input microwave power by

$$\begin{aligned} N_{pn} &= B^2 \\ &= \frac{4\gamma_e}{\gamma^2} B_{in}^2 \\ &= \frac{4\gamma_e}{\gamma^2} N_{in} \\ &= \frac{4\gamma_e}{\gamma^2} \frac{P_{in}}{\hbar\Omega_m}. \end{aligned} \tag{S20}$$

Taking Eq. S19 into Eq. S16, the equation of motion for the optical mode is re-written as

$$\dot{a} = -\left(i\Delta + \frac{\kappa}{2}\right) a - iG\, 2\cos\left(\Omega_d t\right) a + \sqrt{\kappa_e} a_{in}, \tag{S21}$$

where $G = g_0 B$ is the frequency shift of optical mode due to the acoustic field that is present.

B. Optical transmission with active acoustic driving

We numerically solve Eq. S21 to investigate the optical transmission spectra with various microwave input powers. We note that the Eq. S21 assumes a weak optical input and a linear acoustic resonator. The normalized optical transmission T under a continuous optical pump a_{in} is given by

$$T = \left|a_{in} - \sqrt{\kappa_e} a\right|^2 / \left|a_{in}\right|^2. \tag{S22}$$

As the optical mode is being modulated by an acoustic mode at microwave frequency Ω_d, the optical transmission T is expected to associate an oscillation at the same as well as higher order frequencies due to nonlinearity. However, in experiment, the optical transmission spectra are captured by a low frequency (10 MHz) data acquisition card, which does not respond to gigahertz frequencies. Numerically, we use an average to calculate the quasi-DC component of the optical transmission using

$$T_{DC} = \frac{1}{\Delta t}\int_{t_1}^{t_1+\Delta t} d\tau T(\tau), \tag{S23}$$

where time t_1 is set to be greater than the initial stabilization time in numerical calculation of a, and the average time window Δt is chosen to be the integer periods of the driving signal, i.e. N/Ω.

The numerically-calculated optical transmission spectra (Fig. S3) exhibit sidebands in agreement with the experimental measurements in Fig. 3 in the main text.

C. S parameter of acousto-optic cavity

The parameter S_{21} is defined as the normalized microwave power generated by the receiving photodetector, which is generated by beating the pump laser and the optical sideband at the photodetector. To derive the power in the optical sideband, we decompose the optical amplitude a into a series of sidebands:

$$a = \sum_q A_q e^{-iq\Omega_d t}, \tag{S24}$$

where A_q is the amplitude of optical sideband of order q. At the weak microwave input power (i.e. $G \ll \kappa$) limit and in the sideband resolved regime (i.e. $\Omega_m \gg \kappa$), we only consider the first order of optical sidebands, i.e. $q = 0, \pm 1$ and, for simplicity,

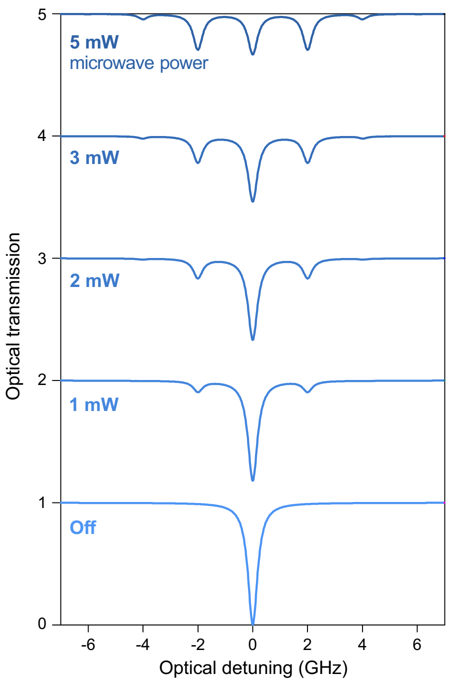

Fig. S3. Numerically calculated optical transmission spectra of acousto-optic cavity with microwave input powers from 0 to 5 mW.

we write the amplitude as, A_0, A_+, A_-. The Eq. S21 is thus decomposed into sidebands,

$$\begin{aligned} 0 &= -\left(i\Delta + \frac{\kappa}{2}\right) A_0 - iG\left(A_+ + A_-\right) + \sqrt{\kappa_e} A_{in} \\ -i\Omega_m A_+ &= -\left(i\Delta + \frac{\kappa}{2}\right) A_+ - iGA_0 \\ i\Omega_m A_- &= -\left(i\Delta + \frac{\kappa}{2}\right) A_- - iGA_0, \end{aligned} \tag{S25}$$

where A_{in} is the input optical amplitude. The solution of Eq. S25 is given by

$$\begin{aligned} A_0 &= \frac{\sqrt{\kappa_e} A_{in}}{\left(i\Delta + \kappa/2 + G^2\left(\frac{1}{i(\Delta-\Omega_d)+\kappa/2} + \frac{1}{i(\Delta+\Omega_d)+\kappa/2}\right)\right)} \\ &\simeq \frac{\sqrt{\kappa_e} A_{in}}{(i\Delta + \kappa/2)} \end{aligned} \tag{S26}$$

$$A_+ = \frac{-iGA_0}{i\left(\Delta - \Omega_d\right) + \kappa/2} \tag{S27}$$

$$A_- = \frac{-iGA_0}{i\left(\Delta + \Omega_d\right) + \kappa/2} \tag{S28}$$

For the scenario the pumping laser is blue detuned from the optical resonance by the acoustic resonant frequency ($\Delta = -\Omega_m$), and the microwave input is on resonant with the acoustic mode ($\Omega_d = \Omega_m$), the in-cavity optical amplitude for the enhanced sideband A_- is given by,

$$A_- = \frac{-iG\sqrt{\kappa_e} A_{in}}{(-i\Omega_m + \kappa/2)\,\kappa/2}, \tag{S29}$$

where acousto-optic coupling strength $G = g_0 B = 2g_0 B_{in}\sqrt{\gamma_e}/\gamma$.

Since the pump laser is detuned from the resonant, the transmitted amplitude of the pump laser is close to the input A_{in}. The output microwave voltage U from the photodetector caused by the beating between the transmitted pump laser and the generated optical sideband given by

$$\begin{aligned} U &= R_{PD}\, \hbar\omega \left|\sqrt{\kappa_e} A_- A_{in}\right| \\ &= R_{PD} \frac{G\kappa_e I_{opt}}{\kappa\sqrt{\Omega_m^2 + \kappa^2/4}/2} \\ &\simeq R_{PD} \frac{G\kappa_e I_{opt}}{\Omega_m \kappa/2}, \end{aligned} \tag{S30}$$

where optical power $I_{opt} = \hbar\omega_0 A_{in}^2$, ω_0 is the optical frequency, and R_{PD} is the response of the photodetector in the unit of V/W. The output microwave power is then given by

$$\begin{aligned} P_{out} &= \frac{U^2}{2R_{load}} \\ &= \frac{2G^2\kappa_e^2 R_{PD}^2 I_{opt}^2}{\Omega_m^2 \kappa^2 R_{load}}, \end{aligned} \tag{S31}$$

where $R_{load} = 50\ \Omega$ is the impedance of the network analyzer. The opto-acoustic transmission S_{21} is given by

$$\begin{aligned} S_{21} &= P_{out}/P_{in} \\ &= \frac{8g_0^2\gamma_e\kappa_e^2 R_{PD}^2 I_{opt}^2}{\hbar\gamma^2\Omega_m^3\kappa^2 R_{load}} \end{aligned} \tag{S32}$$

D. Estimation of acousto-optic single-photon coupling strength g_0 from experimental measurements

Using the experimental results of the acousto-optic cavity (Fig. 3 in the main text), we can extract the single-photon coupling strength g_0 using Eq. S32. Taking the insertion loss of the chip into account, the input optical power I_{opt} in Eq. S32 is replaced by the power received at the photodetector I_{rec}.

We extract the acousto-optic coupling strength $g_0 = 1.1$ kHz from the experimental results shown in Fig. 3 and summarized in Table S2. We note this experimentally-extracted g_0 is in good agreement with the numerically-simulated value (TE mode, 2.17 GHz) in Table S1. The discrepancy of the acoustic resonant frequency between the numerical simulation and experimental measurement may due to the deviation in LN film thickness and etching depth in fabrication.

E. Photon number conversion efficiency

The photon number conversion efficiency η relates the number of generated optical sideband photons coupled out of the cavity $\sqrt{\kappa_e}A_-$ to the input microwave photons. For weak microwave input signals, the conversion efficiency η is given by

$$\begin{aligned} \eta &= \left|\frac{\sqrt{\kappa_e}A_-}{B_{in}}\right|^2 \\ &= \frac{16g_0^2\gamma_e\kappa_e^2 I_{\rm opt}}{\hbar\omega_0\Omega_m^2\gamma^2\kappa^2} \\ &= \frac{4g_0^2}{\gamma\kappa} \cdot \frac{\kappa_e I_{\rm opt}}{\Omega_m^2\hbar\omega_0} \cdot \frac{2\gamma_e}{\gamma} \cdot \frac{2\kappa_e}{\kappa} \\ &= C_0 \cdot n_{\rm cav} \cdot \frac{2\gamma_e}{\gamma} \cdot \frac{2\kappa_e}{\kappa}, \end{aligned} \tag{S33}$$

where $C_0 = 4g_0^2/(\gamma\kappa)$ is the single-photon cooperativity, $n_{\rm cav} = \kappa_e I_{\rm opt}/(\Omega_m^2\hbar\omega_0)$ is the intracavity photon number of the blue-detuned pump light, $2\kappa_e/\kappa$ is the external coupling efficiency of the optical mode, and $2\gamma_e/\gamma$ is the external coupling efficiency of acoustic mode by the IDT.

Using the experimentally-extracted values summarized in Table S2, we estimate a single-photon cooperativity of $C_0 = 4 \times 10^{-8}$. At an optical power of 1 mW, where the intracavity photon number is only about 4,400 due to the large detuning of $\Delta = -\Omega_m$ from the optical resonance, the photon number conversion efficiency is $\eta = 0.0017\%$.

Table S2. Estimation of acousto-optic single-photon coupling strength g_0 using experimental results

Parameter	Value
Optical mode	TE
$\omega_0/2\pi$	200 THz
$\kappa/2\pi$	95 MHz
$2\kappa_e/\kappa$	0.3
$\gamma/2\pi$	1.28 MHz
$2\gamma_e/\gamma$	0.34
$\Omega_m/2\pi$	2.007 GHz
R_{PD}	800 V/W
I_{rec}	0.128 mW
R_{load}	50 Ω
S_{21}	-7.5 dB
$g_0/2\pi$	**1.1 kHz**

4. MICROWAVE MICROSCOPY OF ACOUSTIC MODES

We experimentally investigate the acoustic mode profiles using transmission-mode microwave impedance microscopy [7, 8]. The working principle is the following – while the acoustic resonator is driven by a microwave input on the IDT, a probe for atomic force microscopy is scanning over the acoustic resonator and measuring any microwave electric signals. The detected signal is mixed with the driving signal to extract the relative amplitude and phase of the acoustic electric field. The electric amplitude profile of an acoustic mode is obtained on the top surface and in agreement with the numerical simulation (Fig. S4).

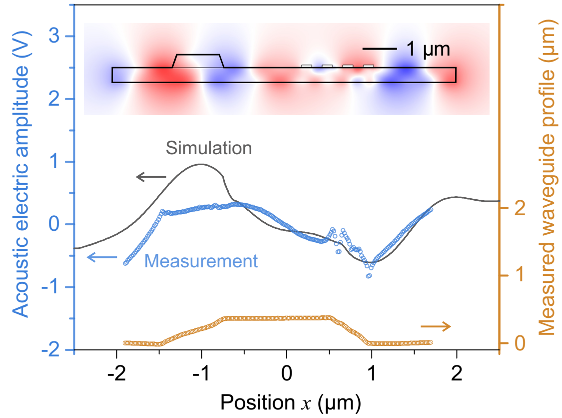

Fig. S4. Electric and topographic profiles of an acoustic mode. The electric field amplitude is detected by a scanning probe using transmission-mode microwave impedance microscopy, with a driving signal at 2 GHz on the acoustic resonance. Inset: simulated electric field amplitude profile of the acoustic mode.

REFERENCES

1. M. J. Burek, J. D. Cohen, S. M. Meenehan, N. El-Sawah, C. Chia, T. Ruelle, S. Meesala, J. Rochman, H. A. Atikian, M. Markham, D. J. Twitchen, M. D. Lukin, O. Painter, and M. Lončar, "Diamond optomechanical crystals," Optica **3**, 1404 (2016).
2. K. C. Balram, M. Davanço, J. Y. Lim, J. D. Song, and K. Srinivasan, "Moving boundary and photoelastic coupling in gaas optomechanical resonators," Optica **1**, 414–420 (2014).
3. M. Eichenfield, J. Chan, R. M. Camacho, K. J. Vahala, and O. Painter, "Optomechanical crystals," Nature **462**, 78 (2009).
4. R. E. Newnham, *Properties of materials: anisotropy, symmetry, structure* (Oxford University Press, New York, 2005).
5. R. S. Weis and T. K. Gaylord, "Lithium niobate: Summary of physical properties and crystal structure," Appl. Phys. A **37**, 191–203 (1985).
6. L. Marculescu and G. Hauret, "Étude de l'effet brillouin à température ordinaire dans le niobate de lithium," Compt. Rend. Acad. Sci. (B) **276**, 555–558 (1973).
7. L. Zheng, H. Dong, X. Wu, Y.-L. Huang, W. Wang, W. Wu, Z. Wang, and K. Lai, "Interferometric imaging of nonlocal electromechanical power transduction in ferroelectric domains," Proc. Natl. Acad. Sci. **115**, 5338–5342 (2018).
8. L. Zheng, D. Wu, X. Wu, and K. Lai, "Visualization of surface-acoustic-wave potential by transmission-mode microwave impedance microscopy," Phys. Rev. Appl. **9**, 061002 (2018).